Article

Combating Biofilms by a Self-Adapting Drug Loading Hydrogel

Xia Li, Ya-nan Fu, Lifei Huang, Fang Liu, Thomas Fintan Moriarty, Lei Tao, Yen Wei, and Xing Wang*

Cite This: https://doi.org/10.1021/acsabm.1c00540
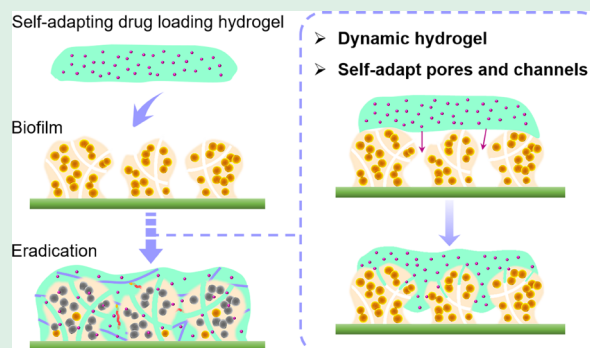
Read Online

ACCESS | Metrics & More | Article Recommendations | Supporting Information

ABSTRACT: A bacterial biofilm is one of the main reasons that many diseases are difficult to cure. Herein, a teicoplanin (TPN)-loaded self-adapting chitosan-based hydrogel (CPH) system, called TPN-CPH, was prepared by encapsulating antibacterial TPN into CPH. This TPN-CPH can effectively combat preformed biofilms *in vitro* of *Staphylococcus aureus* (*S. aureus*). It has a good therapeutic effect on full-thickness cutaneous wounds *in vivo* of mice infected with biofilms. In addition, TPN-CPH can accelerate wound healing by self-adapting the wound and providing a moist environment. The operation process of TPN-CPH is simple, and no external stimulation such as light and heat is needed in the treatment process, making it more convenient for clinical application. Furthermore, this is a challenge to use self-adapting hydrogels to adapt the micro-size channels of biofilms. TPN-CPH provides a chitosan-based self-adapting hydrogel system for loading drugs to kill bacteria in biofilms, and thus it is promising for infection control.

KEYWORDS: hydrogel, drug delivery, self-adapting, biofilm, antibacterial

INTRODUCTION

In recent years, scientists believe that most human bacterial infections are related to bacterial biofilms, especially those chronic and refractory infections.[1−9] In the process of growth and reproduction, bacteria secrete a large amount of extracellular polymeric substances (EPS) such as polysaccharides, proteins, extracellular DNA, and phospholipids, which encapsulate bacteria to form biofilms.[10,11] When the biofilm matures or is stimulated by the environment, some biofilms will disperse and bacteria will spread and colonize to new surfaces. These dispersed bacteria have high toxicity and pose intrinsic risks to acute infection.[12] Those bacteria in the formed biofilm are different from planktonic bacteria; they have extremely strong resistance to harsh environments, host immune defense mechanisms, and bactericides such as antibiotics.[13,14] Therefore, general antibiotic treatment has poor effects on bacterial infection related to biofilms. How to effectively remove biofilms is a major challenge for human being.

Scientists have developed many strategies to fight bacterial biofilms.[15−19] Among them, some methods have been specifically used to inhibit the formation of biofilms.[20−24] These methods either use small-molecule organic compounds to inhibit the surface adhesion of bacteria at the initial stage and interfere with the quorum sensing system or use specific pathway inhibitors to inhibit the synthesis of second nucleotide messenger molecules and the maturation of biofilms.[25−31] However, the biofilm infection that has already occurred is inevitable, so researchers have also designed some strategies to combat the preformed biofilm. Common methods of destroying preformed biofilms include electrochemical methods and the use of antibacterial components with anti-biofilm activity, biomolecules capable of degrading extracellular polymers, and drug delivery systems to destroy mature biofilms.[12,32−39]

Hydrogels have been widely applied in biomedicine[40−44] due to their high hydrophilicity, permeability, and biocompatibility.[45−47] Zhang et al.[48] prepared a multiresponse, dynamic, and self-healing chitosan-based hydrogel by reacting aldehyde groups on dibenzaldehyde-terminated telechelic poly(ethylene glycol) with amino groups on chitosan to form Schiff base bonds. Using the hydrogel as a delivery carrier, the encapsulation and controlled release of rhodamine B and lysozyme were successfully achieved. They then obtained a magnetic self-healing hydrogel by mixing Fe_3O_4 nanoparticles into the hydrogel,[49] which could squeeze through a narrow channel by shape transformation under the assistance of an external magnetic field. Furthermore, Li et al.[50] found that the hydrogel can change shape and move autonomously under natural conditions because its dynamic Schiff base network allows the hydrogel to move like a very viscous fluid. However, so far, the smallest pore size that self-healing hydrogels can
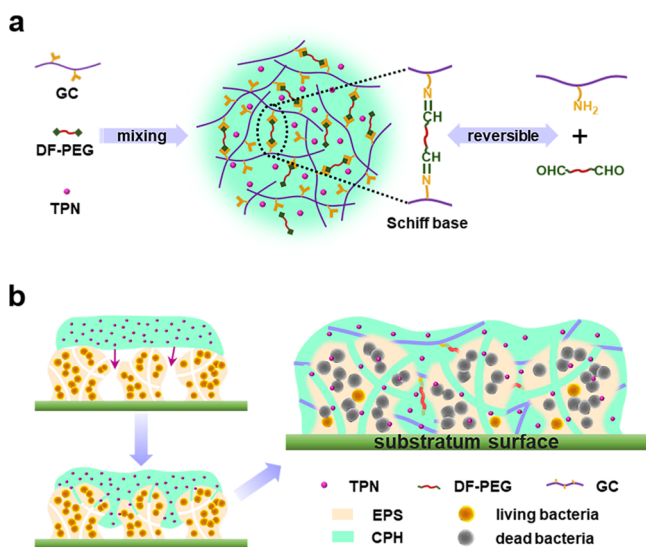
spontaneously penetrate is still unknown, which is a scientific problem to be explored. As we know, there are many pores and channels into the bacterial biofilm so that cells deep within the biofilm can receive nutrients and oxygen and expel wastes.[10] Up to now, it is still not clear what the specific size of channels is in biofilms. However, a few literature studies reported that the size of these pores ranges from 10 nm up to more than 10 μm.[51,52] Therefore, we assume that self-adapting hydrogels can infiltrate the biofilms from those pores and channels. Thus, it can be used as a drug carrier to combat biofilms. Herein, a glycopeptide antibiotic, teicoplanin (TPN), was loaded into a self-adapting chitosan-based hydrogel (CPH) to obtain the TPN-CPH system to verify the above hypothesis (Scheme 1).

Scheme 1. (a) Illustration of the Synthesis and Structure of CPH. (b) Self-Adaptability and Bactericidal Mechanism of CPH, where Self-Adapting Hydrogels Can Infiltrate the Biofilm from Those Pores and Channels

RESULTS

Preparation and Characterizations of CPH. The CPH was prepared by mixing 3% (w/w) glycol chitosan aqueous solution and 1% (w/w) DF-PEG$_{4000}$ aqueous solution in a volume ratio of 3:1. Under this condition, the gelation time was about 10 min (Figure 1a). It indicated that the CPH was successfully prepared through cross-linking of GC with the linker DF-PEG. A porous network structure (Figure 1b) could be clearly observed using a scanning electron microscope (SEM). These porous structures greatly increase the specific surface area inside the hydrogel so that hydrophilic groups can quickly make contact with water molecules, further increasing water content of the hydrogel.

A series of CPH with different solid contents were prepared to analyze their rheological properties. As shown in Figure 1c, the storage modulus (G') value of CPH is about 280 Pa, which is lower than that of the CPH1 hydrogel (about 560 Pa). This suggests that with the increase in the content of DF-PEG, the cross-linking degree of the hydrogel was increased and the mechanical strength was enhanced. That means that the mechanical strength of CPH can be easily adjusted by changing the amount of DF-PEG.

The self-adaptability of CPH was also verified according to the method in the previous literature.[49] CPH could change its shape spontaneously under the action of gravity, passing through those gaps formed among glass beads and finally reaching the bottom of the vial after 24 h (Figure 1d). However, most of the reduced hydrogel in the control group was still above the beads, and there was no obvious shape change compared with the CPH. The main reason for this phenomenon is the existence of dynamic Schiff base bonds in CPH. These Schiff base bonds are continuously in the alternate process of chemical bond formation and breaking, coupled with the driving action of gravity and surface tension. These factors prompted CPH to change its shape to adapt to uneven surfaces, showing excellent self-adaptability.
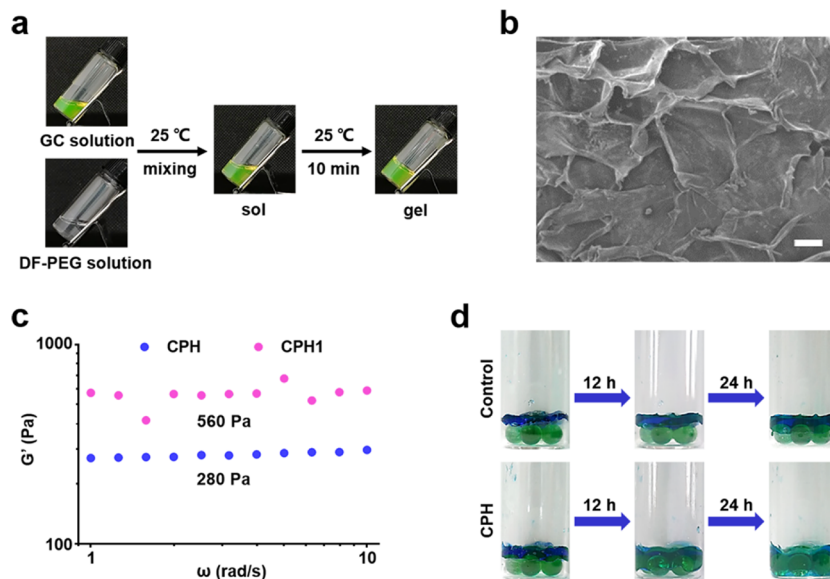

Figure 1. Characterizations of the self-adapting CPH. (a) Preparation process of CPH. The GC solution was stained with FITC for better observation. (b) SEM picture of the CPH microstructures (the bar is 100 μm). (c) Storage modulus (G') of CPH with different solid contents (strains: 1%, 25 °C). The solid content of CPH was 2.5%, and that of CPH1 was 2.75%. (d) Self-adaptability of CPH. CPH reduced by NaBH$_3$CN was used as a control.

***In Vitro* Antibacterial Test.** It was founded that TPN had a good antibacterial effect on *Staphylococcus aureus* (*S. aureus*), and the minimum inhibitory concentration was 1 μg mL^{-1} (Figure S2). Then, TPN-CPH was obtained by loading TPN into CPH, its antibacterial activity was evaluated by inhibition zone experiments, and the results are shown in Figure 2a. In
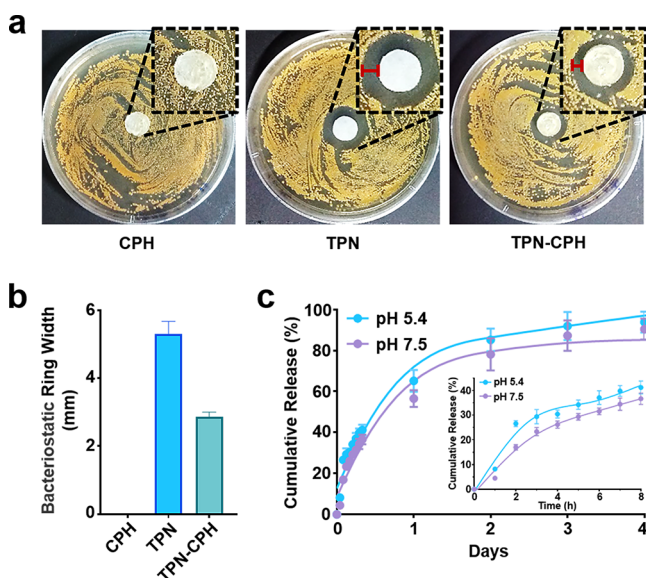

Figure 2. (a) Inhibition zone experiments of CPH, TPN, and TPN-CPH. The red mark in the figure represents the width of the bacteriostatic ring. (b) Quantitative results of the width of the antibacterial ring in different groups (*n* = 3 for each group). (c) Cumulative release profiles of TPN from CPH in PBS solutions with different pH levels (*n* = 3 for each pH value).

the CPH group, there was no antibacterial ring around the material, indicating that CPH alone did not have antibacterial activity. However, it is obvious that both the TPN group and the TPN-CPH group have antibacterial rings. Among them, the inhibition effect of the TPN group was the most obvious, the width of the inhibition ring was about 5.29 mm, and that of the TPN-CPH group was about 2.86 mm (Figure 2b). These results showed that TPN-CPH could release TPN effectively and produce an obvious antibacterial effect on *S. aureus.*

To further study the *in vitro* release of TPN from TPN-CPH, the cumulative release of TPN under different pH conditions was measured (Figure 2c). The figure shows that the release rate of TPN is relatively fast on the first day and then gradually slows down. In general, TPN has the characteristics of continuous release in this CPH carrier system. On the fourth day, the cumulative release of TPN in the pH 7.5 phosphate buffer saline (PBS) reached 90.44%, and that in the pH 5.4 PBS was 93.88%. In addition, the release rate of TPN at pH 7.5 was slightly slower than that at pH 5.4. The reason for this phenomenon is that the CPH is a cross-linked Schiff base, which is itself weakly alkaline. It is favorable for the degradation of CPH under acidic conditions. Therefore, TPN releases faster under pH 5.4.

Combating Biofilms by TPN-CPH *In Vitro*. In order to explore the bactericidal effect of TPN-CPH on bacteria in biofilms, mature *S. aureus* biofilms were treated with PBS, CPH, TPN, and TPN-CPH respectively *in vitro*, and the results are shown in Figure 3. In the PBS group, the red fluorescence was quite weak, suggesting that there were very
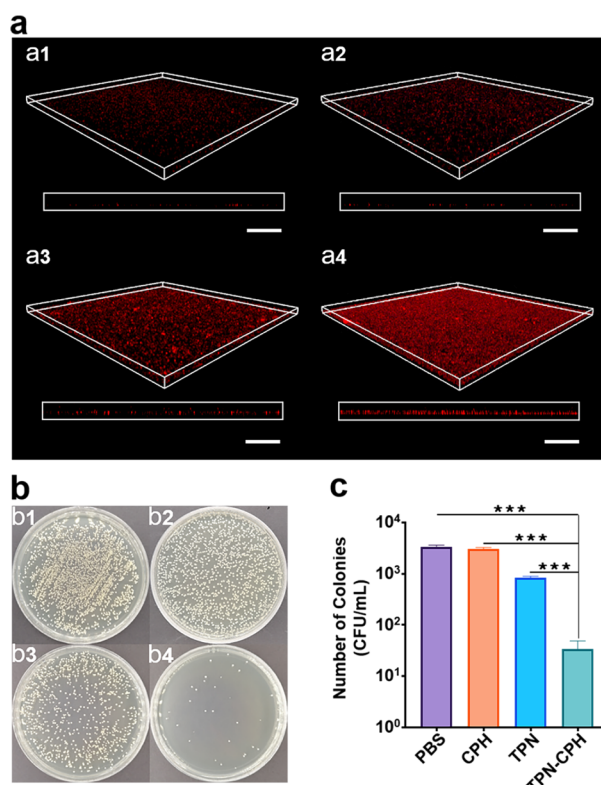

Figure 3. Combating activity of different groups against *S. aureus* biofilms *in vitro*. (a) CLSM images of bacterial biofilms after being treated with PBS (a1), CPH (a2), TPN (a3), and TPN-CPH (a4). The dead bacteria in biofilms were stained red by PI. The bar is 50 μm. (b) Surviving bacteria in biofilms after treating with PBS (b1), CPH (b2), TPN (b3), and TPN-CPH (b4). (c) Colony count results of each group in (b) (*n* = 3 for each group). Significant differences among different groups are specifically marked: ***p < 0.001.

few naturally dead bacteria in the biofilm. The red fluorescence intensity in the CPH group was similar to that in the PBS group, indicating that CPH itself had no obvious antibacterial effect against *S. aureus* in biofilms. Compared with above two groups, the red fluorescence intensity in the TPN solution group and the TPN-CPH group were significantly enhanced. The number of dead bacteria in the biofilm of the TPN-CPH group was the highest. These phenomena indicated that TPN had a certain killing effect on *S. aureus* in biofilms, but it worked weakly, while TPN-CPH could enhance the penetration of TPN in biofilms, thereby producing a better combating effect on biofilms.

The number of viable bacteria surviving in the biofilms was measured, and the results are shown in Figure 3b,c. The colony numbers of the PBS group ($\sim$3343 CFU mL^{-1}) and the CPH group ($\sim$3021 CFU mL^{-1}) were similar, but the TPN group ($\sim$826 CFU mL^{-1}) was obviously lower than the above two groups. Significantly, the TPN-CPH group had the lowest colony number, $\sim$34 CFU mL^{-1}, far lower than other groups. This result is consistent with the result of Figure 3a, indicating that TPN-CPH has a good killing effect on *S. aureus* in biofilms.

Treatment of Full-Thickness Cutaneous Wounds in Mice with Biofilm Infection. To further apply this drug-loaded hydrogel system to treatment *in vivo*, a mouse full-thickness cutaneous wound model with biofilm infection was established successfully and corresponding treatments were

carried out (Figure 4a). Wound healing was studied on days 0, 4, 8, and 12, and the results (Figure 4b,c) showed that the
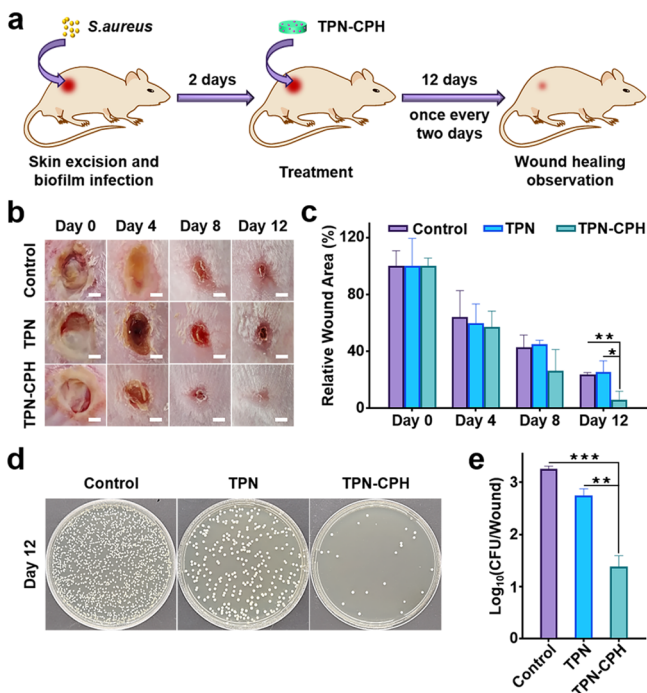

Figure 4. Treatment of biofilm infection of full-thickness cutaneous wound in mice. (a) Schematic representation of experimental process. (b) Wound healing process after treatment in different groups. The bar is 2 mm. (c) Statistical results of the wound healing rate ($n = 6$ for each group). (d, e) Colony count results of skin tissue around the wound after 12 days of treatment ($n = 3$ for each group). The wounds treated with PBS were used as a control group. Significant differences among all the groups are specifically marked: $*p < 0.05$; $**p < 0.01$; $***p < 0.001$.

wounds in all groups were accompanied by extremely serious suppuration on day 0. After 4 days of treatment, the wound suppuration in the control group treated with PBS was still obvious, but the situations in the TPN solution group and the TPN-CPH group were markedly improved, which may be caused by the antibacterial effect of TPN. During the treatment, the wound area of all groups showed a gradual shrinking trend. However, the healing rate of the TPN-CPH group after the eighth day was obviously better than those of other groups. On the 12th day, the wounds in the TPN-CPH group were almost completely healed, which was significantly different from the relative wound areas in other groups. It demonstrated that TPN-CPH is beneficial to wound healing. This may be caused by the fact that TPN-CPH provided a relatively moist environment for the wound, in which wound cells could regenerate and migrate faster due to the self-adapting property of CPH. In other words, in the early stage of treatment, TPN-CPH has a prominent antibacterial effect on *S. aureus*, which leads to the improvement of wound suppuration. In the later stage of treatment, TPN-CPH can create a relatively moist environment for the wound to accelerate the wound healing. Therefore, TPN-CPH has great application value in wound healing.

Living bacteria remaining in the wound tissue after 12 days of treatment were also evaluated, and the results are shown in Figure 4d,e. It can be seen from the results that the number of

colonies in the control group ($\sim$1830 CFU mL^{-1}), the TPN group ($\sim$568 CFU mL^{-1}), and the TPN-CPH group ($\sim$34 CFU mL^{-1}) decreased in turn; among them, the TPN-CPH group was the least. This result verified the bactericidal ability of TPN-CPH on *S. aureus* in the biofilm of cutaneous wounds, which echoed the results *in vitro* and provided a powerful experimental verification *in vivo*.

Evaluation of Biocompatibility. Biomedical materials should have good biocompatibility, so the cytotoxicity of GC, DF-PEG, and TPN to mouse fibroblast cells (L929) was tested (Figure S5a,c). The results showed that the cell viability of the GC solution group was greater than 90% within a concentration range of 1−16 mg mL^{-1}, and that of the DF-PEG solution group was greater than 85% within a concentration range from 0.125 to 2 mg mL^{-1}. This indicated that GC and DF-PEG showed excellent cytocompatibility to L929 cells, suggesting that CPH as a drug carrier would not cause great toxic and side effects to cells. However, TPN solution had relatively greater cytotoxicity to L929 cells, and the cell viability was less than 80% after 24 h of co-cultivation. The cytocompatibilities of extracts of CPH and TPN-CPH were also tested and compared with TPN. The results are shown in Figure 5a. After 24 h of co-cultivation, the cell
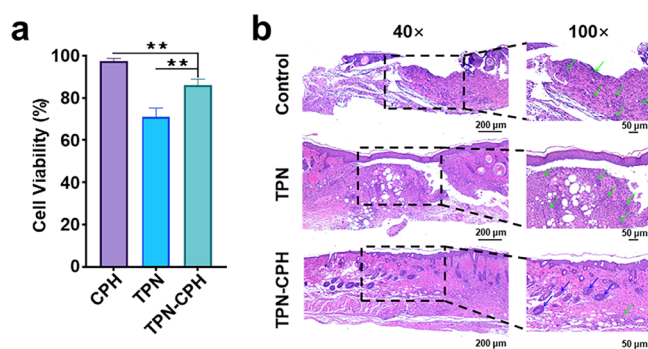

Figure 5. (a) Comparison of the cytotoxicity of CPH, TPN, and CPH-TPN to L929 cells ($n = 4$ for each group). Significant differences among all the groups are specifically marked: $**p < 0.01$. (b) H&E staining of mouse skin wound tissues in different groups after 12 days of treatment. Wound tissue treated with PBS was used as a control group. Green arrows point to inflammatory cells. Blue arrows point to hair follicles.

viability of the CPH group was about 97%, while that of the TPN group was only 70%. Interestingly, the cell viability of the TPN-CPH group was as high as 86%, which was much higher than the TPN group. The main reason for this result was that the actual concentration of TPN in the TPN-CPH group was lower than that in the TPN solution group due to the slow-release effect of CPH on TPN. Therefore, loading TPN into CPH was beneficial to reduce the cytotoxicity of TPN and ensured that TPN-CPH had good cell compatibility with L929 cells.

Furthermore, H&E staining was also performed on mouse skin wound tissues in different groups after 12 days of treatment to evaluate wound healing and the *in vivo* biocompatibility of different materials (Figure 5b). From the staining results, it was not difficult to find that the skin epidermis in the control group had obvious discontinuities, and a large number of inflammatory cells infiltrated among the dense fibrous tissues of the dermal reticular layer, mainly lymphocytes. In the TPN solution group and the TPN-CPH

group, the wound tissue was covered by intact squamous epithelium, accompanied by hyperkeratosis and insufficiency, and the keratinized layer was loose. However, in the TPN solution group, more inflammatory cells infiltrated the dermal fibrous tissue, and there were very few hair follicles. In contrast, the infiltrating inflammatory cells in the TPN-CPH group were significantly reduced, and there were more hair follicles and sebaceous glands, which indicated that TPN-CPH had better biocompatibility *in vivo* and was more beneficial to wound healing.

Mechanism Speculation of TPN-CPH in Treating Biofilm Infection. Based on all the above experimental results, the mechanism of TPN-CPH killing *S. aureus* in biofilms was speculated. There are a lot of Schiff base bonds in TPN-CPH, which are unstable and in the dynamic process of chemical bond formation and fracture alternately, which shows the change of hydrogel shape macroscopically. When TPN-CPH makes contact with the biofilm, its shape changes under the action of gravity and surface tension, and then it enters the biofilm through the pores and channels on the biofilm. As we know, the biofilm is acidic (pH < 6). Under this condition, TPN-CPH will accelerate degradation and release more TPN to act on bacteria, thus achieving a better combating effect on biofilms.

CONCLUSIONS

In summary, the TPN-CPH system was successfully prepared with a simple method. The drug-loaded hydrogel system has good self-adaptability, degradability, and biocompatibility. The self-adapting TPN-CPH allows it to adapt to various uneven surfaces and external microstructures by changing its shape. More importantly, this research demonstrated that the TPN-CPH could enter the pores of the biofilm. One reason is its self-adaptability, and the other is that TPN-CPH itself is weakly alkaline. Under the acidic conditions inside the biofilm, CPH is accelerated to release more TPN to act on inner *S. aureus*, thereby producing a better combating effect on the biofilm. In addition, TPN-CPH can create a relatively moist environment for cutaneous wounds, which can promote cell regeneration and speed up cell migration to accelerate wound healing. These outstanding characteristics make TPN-CPH promising in the treatment of diseases related to biofilm infections.

EXPERIMENTAL SECTION

Reagents and Chemicals. Glycol chitosan (Wako Pure Chemical Industries, 90% degree of deacetylation, Mn $\approx$80,000 up) and PEG (Sinopharm Chemical Reagent, Mn $\approx$4000) were used as purchased. DF-PEG (Mn $\approx$4000 g mol^{-1}) was synthesized following a procedure in the previous literature.[47] Teicoplanin was ordered from Changchun Yuandaguoao Pharm. All solvents were purchased from Sinopharm Chemical Reagent and used directly without further purification. Other agents were purchased from Sinopharm and used without further purification.

Characterizations. A total of 5 mg of DF-PEG powder was dissolved in 0.6 mL of dimethyl sulfoxide-d_6, and then the ^{1}H NMR spectra of DF-PEG were obtained using a JEOL JNM-ECA400 (400 MHz) spectrometer. The rheology analysis of CPH was carried out using an AR-2 rheometer with parallel plate geometry (20 mm in diameter). In the rheological analysis, "Oscillation Frequency" scanning mode was used. The temperature within two parallel plates was 25 °C. The strain was 1%, and the angular frequency increased from 0.1 to 100 rad/s. The experiment was repeated three times. CPH was freeze-dried and then adhered to the conductive adhesive for gold

spraying. Then, the microstructure of the hydrogel was characterized by SEM (JEOL JSM-7800F, JEOL, Japan). The acceleration voltage used for the SEM analysis was 10.0 kV. A Leica CLSM was used to observe the antibacterial effect against *S. aureus* in biofilms.

Synthesis of DF-PEG. DF-PEG was prepared by referring to the method of the previous literature.[49] Briefly, 6.52 g of poly(ethylene glycol) was dissolved in toluene and then the solution was evaporated to dryness on a rotary evaporator to remove water. After that, 3.26 g of 4-carboxybenzaldehyde was added followed by 1.68 g of DCC as a dehydrating agent and 0.05 g of DMAP as a catalyst. Finally, 30 mL of tetrahydrofuran was added as a solvent to completely dissolve reactants. The reaction was stirred at room temperature for 24 h. Afterward, the mixture obtained after the reaction was filtered. The collected filtrate was dropped into ether for precipitation to wash impurities. The purification process was repeated three times. Finally, the white solid DF-PEG was obtained through vacuum drying for 24 h.

Preparation of CPH. A 3% wt GC solution, 2% wt DF-PEG solution, and 1% wt DF-PEG solution were prepared by dissolving GC and DF-PEG in deionized water. Then, 1% wt DF-PEG solution and 3% wt GC solution were mixed evenly at a volume ratio of 1:3 for 10−20 min to obtain CPH. A 2% wt DF-PEG solution and 3% wt GC solution were mixed at a volume ratio of 1:3 to obtain CPH1.

Preparation of TPN-CPH. TPN was dissolved in a 3% wt glycol chitosan solution to obtain TPN-GC solution. Then, TPN-GC solution was mixed with a 1% wt DF-PEG solution evenly at a volume ratio of 3:1 to result in gelation.

Mechanical Strength of CPH. Typically, a piece of hydrogel (∼1 mL, 20 mm diameter) was put on the measuring plate of a rheometer. The storage modulus (G') of the hydrogel was recorded under different frequencies (strains: 1%, 25 °C). All hydrogels were tested through the same process.

Self-Adapting Property Test of CPH. According to the method in the literature with slight modification, the self-adaptability of CPH was studied. In short, a layer of glass beads (diameter: 4 mm) was put on the bottom of a vial to create an uneven surface. Gaps were formed among these small glass beads. Then, the hydrogel sheet was put on top of these small balls and it was observed whether the hydrogel will pass through those gaps to the bottom of the vial. The hydrogel reduced by NaBH$_3$CN was used as a control.

***In Vitro* Release of TPN.** First, 1 mL of GC/DF-PEG mixed solution containing TPN was added into a 10 mL centrifuge tube to form a hydrogel. Next, 5 mL of PBS buffer solution was added as a release medium. The tube was placed on a constant temperature shaker at 37 °C and 180 rpm. At predetermined intervals, 3.0 mL of the release medium was taken out and immediately replaced with the same volume of fresh PBS solution. The OD value of the collected liquid at 279 nm was measured using an ultraviolet spectrophotometer.

***In Vitro* Biocompatibility Studies.** The biocompatibility study was carried out with L929 cells. L929 cells were cultured in a 96-well plate from an initial inoculum of 8×10^3 cells in each well. The cells were cultured in RPMI-1640 supplemented with 10% fetal bovine serum, 5% penicillin−streptomycin, and incubated at 37 °C in an incubator with 5% CO$_2$ for 24 h to make them adhere to the wall followed by removing the medium in each well and adding 100 μL of extract solutions of CPH, TPN solution, and extract solutions of TPN-CPH. The 96-well plate was placed in an incubator and incubated for a total of 24 h. The 96-well plate was put into the incubator for another 24 h. After that, 10 μL of MTT dye was added to each well and incubated for 4 h at 37 °C. A total of 100 μL of SDS was added to each well to dissolve formazan crystals. The plate was then analyzed with a microplate reader. Measurements of dye absorbance were carried out at 570 nm. Wells containing only cells and culture medium served as controls. Six replicate wells were used for each group, and the experiment was repeated three times. GC, DF-PEG, and TPN were also assayed using the same method (Figure S5).

Preparation of Bacterial Suspension. The *S. aureus* ATCC 25923, obtained from the American Type Culture Collection, were inoculated on a tryptone soybean agar (TSA) solid culture medium

by an inoculation ring and were incubated at 37 °C for 20 h. A single colony of *S. aureus* on the TSA plate was transferred to tryptone soy broth (TSB) liquid culture medium and incubated overnight with shaking at 37 °C. After that, bacterial solutions were centrifuged at 6000 rpm for 6 min to collect the bacteria followed by washing three times with 0.9% NaCl solution. Finally, the concentration of the bacterial suspension was adjusted to around 1×10^9 CFU mL^{-1}.

Minimum Inhibitory Concentration (MIC) of TPN. TPN stock solution with a concentration of 1280 μg mL^{-1} was serially diluted with TSB culture medium so that the final concentrations of TPN in each well of the 96-well plate were 64, 32, 16, 8, 4, 2, 1, 0.5, 0.25, and 0.125 μg mL^{-1}. Then, 100 μL of 1×10^6 CFU mL^{-1} *S. aureus* suspension was added into each well. Also, the *S. aureus* suspension and TSB medium without TPN were, respectively, used as the positive control group and negative control group. It was repeated three times per well. Finally, the 96-well plate was placed in the bacteria incubator to incubate for 20 h at 37 °C. The OD value at 590 nm was measured using a microplate reader.

In Vitro Antibacterial Activity of TPN, CPH, and TPN-CPH. After the *S. aureus* suspension was prepared by the method described above, it was diluted with PBS to 1×10^6 CFU mL^{-1}. A total of 100 μL of diluted bacterial suspension was taken and coated on TSA culture media using a glass coating rod. Then, sterile filter papers were attached to the center of TSA plates. A total of 100 μL of TPN solution, CPH, and TPN-CPH was next placed on sterile filter papers. These plates were cultured in the bacteria incubator to incubate for 20 h. Photos were taken, and the width of the bacteriostatic ring was measured.

Culture of S. aureus Biofilms. Biofilms were cultured referring to the method in the literature[53] with a slight modification. In order to culture biofilms, the *S. aureus* ATCC 25923 suspension was obtained by the method in the "Preparation of Bacterial Suspension" section. The bacterial suspension was diluted to a concentration of 1×10^8 CFU mL^{-1} with a TSB culture medium. Next, 1 mL of the bacterial suspension above was transferred to each 35 mm laser confocal Petri dish (glass bottom diameter was 20 mm) followed by placing them in the bacteria incubator to incubate for 24 h at 37 °C. Then, culture media were discarded and replaced with new TSB culture media. Then, they were incubated for another 24 h to form mature biofilms. These biofilms were gently washed three times with PBS to remove planktonic bacteria.

Killing S. aureus in Biofilms In Vitro. Mature *S. aureus* biofilms were cultured by the operation described above. Next, these biofilms were further cultured with adding 1 mL of PBS, CPH, TPN, and TPN-CPH on the surfaces at 37 °C for 24 h. Then, propidium iodide (PI) dyes were added to the laser confocal Petri dish to stain dead bacteria in biofilms in the dark for 15 min at room temperature. Excess dyes were discarded by gently washing biofilms three times with PBS. The results were observed using a confocal laser scanning microscope to take photos. Imaris software was used to process the obtained pictures.

According to the previous literature,[54] a colony counting method was used here to quantify living bacteria in biofilms. In short, 100 μL of 1×10^8 CFU mL^{-1} *S. aureus* suspensions diluted by TSB medium was added to each well in a 96-well plate. The suspensions were allowed to grow for 24 h at 37 °C. After replacing the fresh TSB medium, they were cultured for another 24 h to form mature biofilms. Next, 100 μL of PBS, CPH, TPN, and TPN-CPH was added to different wells to treat biofilms for 24 h. Subsequently, those added substances were removed from wells and biofilms were washed 2 times mildly with PBS. Then, 100 μL of PBS were added into each well to sonicate biofilms for 20 min and collect suspensions. These suspensions were serially diluted and spread on TSA plates. The number of colonies was counted after 24 h incubation at 37 °C.

Treatment of Biofilm Infection in the Full-Thickness Cutaneous Wound of Mice. BALB/c mice aged 6−8 weeks (weighing 18−20 g) were purchased from Beijing Vital River Laboratory Animal Technology Co., Ltd. and allowed to acclimatize for 1 week in the laboratory. The experiment was approved by the Animal Ethics Committee of Beijing University of Chemical

Technology. These animals were randomly grouped into three groups with 12 animals per group. Before the experiment, the backs of all mice were shaved using an electric shaver. In order to construct a model of full-thickness cutaneous wound biofilm infection in mice, the mice were anesthetized with sodium pentobarbital. A mouse full-thickness cutaneous wound with a diameter of about 7 mm was made on the back through a skin biopsy punch. After that, 10 μL of *S. aureus* suspension (1×10^8 CFU mL^{-1}) was evenly dispersed into the wound. The infected wound was covered with 3M transparent dressing to prevent contamination by other bacteria. Two days later, the wounds were treated with TPN, CPH, and TPN-CPH, which were applied once every 2 days. After 12 days of treatment, all mice were sacrificed and the skin tissues around these wounds were taken. Parts of these samples were used for colony count, and the other parts were used for histopathological analysis.

■ ASSOCIATED CONTENT

ⓢ Supporting Information

The Supporting Information is available free of charge at https://pubs.acs.org/doi/10.1021/acsabm.1c00540.

■ AUTHOR INFORMATION

Corresponding Author

Xing Wang − *Beijing Laboratory of Biomedical Materials, Beijing University of Chemical Technology, Beijing 100029, P. R. China;* ⓞ orcid.org/0000-0002-9990-1479; Email: wangxing@mail.buct.edu.cn

Authors

Xia Li − *Beijing Laboratory of Biomedical Materials, Beijing University of Chemical Technology, Beijing 100029, P. R. China*

Ya-nan Fu − *Beijing Laboratory of Biomedical Materials, Beijing University of Chemical Technology, Beijing 100029, P. R. China; AO Research Institute Davos, Davos Platz 7270, Switzerland*

Lifei Huang − *Beijing Laboratory of Biomedical Materials, Beijing University of Chemical Technology, Beijing 100029, P. R. China*

Fang Liu − *Department of Gastroenterology, China-Japan Friendship Hospital, Beijing 100029, P. R. China*

Thomas Fintan Moriarty − *AO Research Institute Davos, Davos Platz 7270, Switzerland*

Lei Tao − *The Key Laboratory of Bioorganic Phosphorus Chemistry & Chemical Biology (Ministry of Education), Department of Chemistry, Tsinghua University, Beijing 100084, China;* ⓞ orcid.org/0000-0002-1735-6586

Yen Wei − *The Key Laboratory of Bioorganic Phosphorus Chemistry & Chemical Biology (Ministry of Education), Department of Chemistry, Tsinghua University, Beijing 100084, China;* ⓞ orcid.org/0000-0001-5950-0163

Complete contact information is available at:
https://pubs.acs.org/10.1021/acsabm.1c00540

Author Contributions

The corresponding author X.W. is responsible in ensuring that the descriptions are accurate and agreed upon by all authors. X.L. designed the experiments and carried out material preparation and evaluation, data analysis, and writing the

original draft. Y.F. conducted data analysis and mechanism discussion. L.H. consulted the relevant literature. F.L,, T.F.M., L.T., and Y.W. assisted in evaluating the materials and refining the draft. X.W. conceived and designed the research plan, refined the draft, supervised the project, and contributed to the funding acquisition. All the authors contributed to the interpretation of the results and data analysis and edited the manuscript at all stages.

Notes

The authors declare no competing financial interest.

■ ABBREVIATIONS

TPN, teicoplanin; CPH, chitosan-based hydrogel; GC, glycol chitosan; DCC, *N,N*-dicyclohexylcarbodiimide; DMAP, 4-(dimethylamino)pyridine; CLSM, confocal laser scanning microscopy; EPS, extracellular polymeric substances; SEM, scanning electron microscope; *S. aureus*, *Staphylococcus aureus*; TSA, tryptone soybean agar; TSB, tryptone soy broth; MIC, minimum inhibitory concentration; L929, mouse fibroblast cells; PI, propylene iodide; MTT, 3-(4,5-dimethylazolyl-2)-2,5-diphenyl tetrazolium bromide; SDS, sodium dodecyl sulfate

■ REFERENCES

(1) Conlon, B. P.; Nakayasu, E. S.; Fleck, L. E.; LaFleur, M. D.; Isabella, V. M.; Coleman, K.; Leonard, S. N.; Smith, R. D.; Adkins, J. N.; Lewis, K. Activated ClpP Kills Persisters and Eradicates a Chronic Biofilm Infection. *Nature* **2013**, *503*, 365−370.

(2) Porter, S. L.; Coulter, S. M.; Pentlavalli, S.; Thompson, T. P.; Laverty, G. Self-assembling Diphenylalanine Peptide Nanotubes Selectively Eradicate Bacterial Biofilm Infection. *Acta Biomater.* **2018**, *77*, 96−105.

(3) Milho, C.; Andrade, M.; Boas, D. V.; Alves, D.; Sillankorva, S. Antimicrobial Assessment of Phage Therapy Using a Porcine Model of Biofilm Infection. *Int. J. Pharm.* **2019**, *557*, 112−123.

(4) Dong, Z.; Sun, Y.; Chen, Y.; Liu, Y.; Tang, C.; Qu, X. Injectable Adhesive Hydrogel through a Microcapsule Cross-Link for Periodontitis Treatment. *ACS Appl. Bio Mater.* **2019**, *2*, 5985−5994.

(5) Xi, Y.; Wang, Y.; Gao, J.; Xiao, Y.; Du, J. Dual Corona Vesicles with Intrinsic Antibacterial and Enhanced Antibiotic Delivery Capabilities for Effective Treatment of Biofilm-Induced Periodontitis. *ACS Nano* **2019**, *13*, 13645−13657.

(6) Vestby, L. K.; Gronseth, T.; Simm, R.; Nesse, L. L. Bacterial Biofilm and its Role in the Pathogenesis of Disease. *Antibiotics* **2020**, *9*, 59−87.

(7) Furukawa, S.; Kuchma, S. L.; O'Toole, G. A. Keeping Their Options Open: Acute Versus Persistent Infections. *J. Bacteriol.* **2006**, *188*, 1211−1217.

(8) Römling, U.; Balsalobre, C. Biofilm Infections, Their Resilience to Therapy and Innovative Treatment Strategies. *J. Intern. Med.* **2012**, *272*, 541−561.

(9) de la Fuente-Núñez, C.; Reffuveille, F.; Fernandez, L.; Hancock, R. E. Bacterial Biofilm Development as a Multicellular Adaptation: Antibiotic Resistance and New Therapeutic Strategies. *Curr. Opin. Microbiol.* **2013**, *16*, 580−589.

(10) Flemming, H. C.; Wingender, J. The Biofilm Matrix. *Nat. Rev. Microbiol.* **2010**, *8*, 623−633.

(11) Fulaz, S.; Vitale, S.; Quinn, L.; Casey, E. Nanoparticle−biofilm Interactions: the Role of the EPS Matrix. *Trends Microbiol.* **2019**, *27*, 915−926.

(12) Wolfmeier, H.; Pletzer, D.; Mansour, S. C.; Hancock, R. E. W. New Perspectives in Biofilm Eradication. *ACS Infect. Dis.* **2018**, *4*, 93−106.

(13) Guilhen, C.; Forestier, C.; Balestrino, D. Biofilm Dispersal: Multiple Elaborate Strategies for Dissemination of Bacteria with Unique Properties. *Mol. Microbiol.* **2017**, *105*, 188−210.

(14) Davies, D. Understanding Biofilm Resistance to Antibacterial Agents. *Nat. Rev. Drug Discovery* **2003**, *2*, 114−122.

(15) Zhang, X.; Zhang, G.; Chai, M.; Yao, X.; Chen, W.; Chu, P. K. Synergistic Antibacterial Activity of Physical-chemical Multi-mechanism by TiO$_2$ Nanorod Arrays for Safe Biofilm Eradication on Implant. *Bioact. Mater.* **2021**, *6*, 12−25.

(16) Chen, M.; Zhang, S.; He, Z. Controlled Block Polypeptide Composed of D-Type Amino Acids: A Therapeutics Delivery Platform to Inhibit Biofilm Formation of Drug-Resistant Bacteria. *ACS Appl. Bio Mater.* **2020**, *3*, 6343−6350.

(17) Ran, H.-H.; Cheng, X.; Bao, Y.-W.; Hua, X.-W.; Gao, G.; Zhang, X.; Jiang, Y.-W.; Zhu, Y.-X.; Wu, F.-G. Multifunctional Quaternized Carbon Dots with Enhanced Biofilm Penetration and Eradication Efficiencies. *J. Mater. Chem. B* **2019**, *7*, 5104−5114.

(18) Cao, Z.; Chen, J.; Tran, J.; Chen, X.; Bacacao, B.; Bekale, L. A.; Santa Maria, P. L. Antimicrobial Gold Nanoclusters Eradicate *Escherichia coli* Biofilms and Are Nontoxic by Oral Administration. *ACS Appl. Bio Mater.* **2020**, *3*, 5275−5286.

(19) Rouillard, K. R.; Markovetz, M. R.; Bacudio, L. G.; Hill, D. B.; Schoenfisch, M. H. *Pseudomonas aeruginosa* Biofilm Eradication via Nitric Oxide-releasing Cyclodextrins. *ACS Infect. Dis.* **2020**, *6*, 1940−1950.

(20) Zhang, P.; Li, S.; Chen, H.; Wang, X.; Liu, L.; Lv, F.; Wang, S. Biofilm Inhibition and Elimination Regulated by Cationic Conjugated Polymers. *ACS Appl. Mater. Interfaces* **2017**, *9*, 16933−16938.

(21) Chakraborty, P.; Dastidar, D. G.; Paul, P.; Dutta, S.; Basu, D.; Sharma, S. R.; Basu, S.; Sarker, R. K.; Sen, A.; Sarkar, A.; Tribedi, P. Inhibition of Biofilm Formation of *Pseudomonas aeruginosa* by Caffeine: a Potential Approach for Sustainable Management of Biofilm. *Arch. Microbiol.* **2020**, *202*, 623−635.

(22) Singh, P.; Pandit, S.; Garnæs, J.; Tunjic, S.; Mokkapati, V. R. S. S.; Sultan, A.; Thygesen, A.; Mackevica, A.; Mateiu, R. V.; Daugaard, A. E.; Baun, A.; Mijakovic, I. Green Synthesis of Gold and Silver Nanoparticles from *Cannabis sativa* (Industrial Hemp) and Their Capacity for Biofilm Inhibition. *Int. J. Nanomed.* **2018**, *Volume 13*, 3571−3591.

(23) Besinis, A.; Hadi, S. D.; Le, H. R.; Tredwin, C.; Handy, R. D. Antibacterial Activity and Biofilm Inhibition by Surface Modified Titanium Alloy Medical Implants Following Application of Silver, Titanium Dioxide and Hydroxyapatite Nanocoatings. *Nanotoxicology* **2017**, *11*, 327−338.

(24) Khan, F.; Lee, J.-W.; Pham, D. T. N.; Lee, J.- H.; Kim, H.-W.; Kim, Y.-K.; Kim, Y.-M. Streptomycin Mediated Biofilm Inhibition and Suppression of Virulence Properties in *Pseudomonas aeruginosa* PAO$_1$. *Appl. Microbiol. Biotechnol.* **2020**, *104*, 799−816.

(25) Tetz, G. V.; Artemenko, N. K.; Tetz, V. V. Effect of DNase and Antibiotics on Biofilm Characteristics. *Antimicrob. Agents Chemother.* **2009**, *53*, 1204−1209.

(26) Whitchurch, C. B.; Tolker-Nielsen, T.; Ragas, P. C.; Mattick, J. S. Extracellular DNA Required for Bacterial Biofilm Formation. *Science* **2002**, *295*, 1487−1487.

(27) Kaplan, J. B. Biofilm Dispersal: Mechanisms, Clinical Implications, and Potential Therapeutic Uses. *J. Dent. Res.* **2010**, *89*, 205−218.

(28) Parrino, B.; Diana, P.; Cirrincione, G.; Cascioferro, S. Bacterial Biofilm Inhibition in the Development of Effective Anti-virulence Strategy. *Open Med. Chem. J.* **2018**, *12*, 84−87.

(29) Iwase, T.; Uehara, Y.; Shinji, H.; Tajima, A.; Seo, H.; Takada, K.; Agata, T.; Mizunoe, Y. *Staphylococcus epidermidis* Esp Inhibits

Staphylococcus aureus Biofilm Formation and Nasal Colonization. *Nature* **2010**, *465*, 346−349.

(30) Periasamy, S.; Joo, H.-S.; Duong, A. C.; Bach, T.-H. Y.; Tan, V. Y.; Chatterjee, S. S.; Cheung, G. Y. C.; Otto, M. How *Staphylococcus aureus* Biofilms Develop Their Characteristic Structure. *Proc. Natl. Acad. Sci.* **2012**, *109*, 1281−1286.

(31) Chaignon, P.; Sadovskaya, I.; Ragunah, C.; Ramasubbu, N.; Kaplan, J. B.; Jabbouri, S. Susceptibility of Staphylococcal Biofilms to Enzymatic Treatments Depends on Their Chemical Composition. *Appl. Microbiol. Biotechnol.* **2007**, *75*, 125−132.

(32) Sultana, S. T.; Babauta, J. T.; Beyenal, H. Electrochemical Biofilm Control: a Review. *Biofouling* **2015**, *31*, 745−758.

(33) Freebairn, D.; Linton, D.; Harkin-Jones, E.; Jones, D. S.; Gilmore, B. F.; Gorman, S. P. Electrical Methods of Controlling Bacterial Adhesion and Biofilm on Device Surfaces. *Expert Rev. Med. Devices* **2013**, *10*, 85−103.

(34) Ooi, N.; Eady, E. A.; Cove, J. H.; O'Neill, A. J. *Tert*-butyl Benzoquinone: Mechanism of Biofilm Eradication and Potential for Use as a Topical Antibiofilm Agent. *J. Antimicrob. Chemother.* **2016**, *71*, 1841−1844.

(35) Wang, W.; Peng, R.; Liu, J.; Wang, Z.; Guo, T.; Liang, Q.; Carrier, A. J.; Wang, L.; Zhang, X. Biofilm Eradication by *in situ* Generation of Reactive Chlorine Species on Nano-CuO Surfaces. *J. Mater. Sci.* **2020**, *55*, 11609−11621.

(36) Garrison, A. T.; Abouelhassan, Y.; Kallifidas, D.; Bai, F.; Ukhanova, M.; Mai, V.; in, S.; Luesch, H.; Huigens, R. W., III Halogenated Phenazines that Potently Eradicate Biofilms, MRSA Persister Cells in Non-Biofilm Cultures, and *Mycobacterium tuberculosis*. *Am. Ethnol.* **2015**, *127*, 14819−15036.

(37) Okshevsky, M.; Regina, V. R.; Meyer, R. L. Extracellular DNA as a Target for Biofilm Control. *Curr. Opin. Biotechnol.* **2015**, *33*, 73−80.

(38) Hymes, S. R.; Randis, T. M.; Sun, T. Y.; Ratner, A. J. DNase Inhibits *Gardnerella vaginalis* Biofilms *in vitro* and *in vivo*. *J. Infect. Dis.* **2013**, *207*, 1491−1497.

(39) Forier, K.; Raemdonck, K.; De Smedt, S. C.; Demeester, J.; Coenye, T.; Braeckmans, K. Lipid and Polymer Nanoparticles for Drug Delivery to Bacterial Biofilms. *J. Controlled Release* **2014**, *190*, 607−623.

(40) Zhu, X.; Zhu, Y.; Jia, K.; Abraha, B. S.; Li, Y.; Peng, W.; Zhang, F.; Fan, X.; Zhang, L. A Near-infrared Light-mediated Antimicrobial Based on Ag/Ti$_3$C$_2$T$_x$ for Effective Synergetic Antibacterial Applications. *Nanoscale* **2020**, *12*, 19129−19141.

(41) Zeng, G.; Huang, L.; Huang, Q.; Liu, M.; Xu, D.; Huang, H.; Yang, Z.; Deng, F.; Zhang, X.; Wei, Y. Rapid Synthesis of MoS$_2$-PDA-Ag Nanocomposites as Heterogeneous Catalysts and Antimicrobial Agents via Microwave Irradiation. *Appl. Surf. Sci.* **2018**, *459*, 588−595.

(42) Wang, D.; Wang, J.; Xie, W.; Zhao, W.; Zhang, Y.; Sun, X.; Zhao, L. Drug-loaded Magnetic Microhydrogel as Microwave Susceptible Agents for Cancer Multimodality Treatment and MR Imaging. *J. Biomed. Nanotechnol.* **2018**, *14*, 362−370.

(43) Yang, C.; Xue, R.; Zhang, Q.; Yang, S.; Liu, P.; Chen, L.; Wang, K.; Zhang, X.; Wei, Y. Nanoclay Cross-linked Semi-IPN Silk Sericin/ Poly (NIPAm/LMSH) Nanocomposite Hydrogel: An Outstanding Antibacterial Wound Dressing. *Mater. Sci. Eng., C* **2017**, *81*, 303−313.

(44) Hu, K.; Hu, M.; Xiao, Y.; Cui, Y.; Yan, J.; Yang, G.; Zhang, F.; Lin, G.; Yi, H.; Han, L.; Li, L.; Wei, Y.; Cui, F. Preparation Recombination Humanlike Collagen/Fibroin Scaffold and Promoting the Cell Compatibility with Osteoblasts. *J. Biomed. Mater. Res.* **2021**, *109*, 346−353.

(45) Brown, T. E.; Anseth, K. S. Spatiotemporal Hydrogel Biomaterials for Regenerative Medicine. *Chem. Soc. Rev.* **2017**, *46*, 6532−6552.

(46) Wang, Z.; Ren, Y.; Zhu, Y.; Hao, L.; Chen, Y.; An, G.; Wu, H.; Shi, X.; Mao, C. A Rapidly Self-Healing Host−Guest Supramolecular Hydrogel with High Mechanical Strength and Excellent Biocompatibility. *Am. Ethnol.* **2018**, *57*, 9146−9012.

(47) Pupkaite, J.; Rosenquist, J.; Hilborn, J.; Samanta, A. Injectable Shape-Holding Collagen Hydrogel for Cell Encapsulation and Delivery Cross-linked Using Thiol-Michael Addition Click Reaction. *Biomacromolecules* **2019**, *20*, 3475−3484.

(48) Zhang, Y.; Tao, L.; Li, S.; Wei, Y. Synthesis of Multiresponsive and Dynamic Chitosan-based Hydrogels for Controlled Release of Bioactive Molecules. *Biomacromolecules* **2011**, *12*, 2894−2901.

(49) Zhang, Y.; Yang, B.; Zhang, X.; Xu, L.; Tao, L.; Li, S.; Wei, Y. A Magnetic Self-healing Hydrogel. *Chem. Commun.* **2012**, *48*, 9305−9307.

(50) Li, Y.; Wang, X.; Fu, Y.-n.; Wei, Y.; Zhao, L.; Tao, L. Self-Adapting Hydrogel to Improve the Therapeutic Effect in Wound-Healing. *ACS Appl. Mater. Interfaces* **2018**, *10*, 26046−26055.

(51) Rooney, L. M.; Amos, W. B.; Hoskisson, P. A.; McConnell, G. Intra-colony Channels in *E. coli* Function as a Nutrient Uptake System. *ISME J.* **2020**, *14*, 2461−2473.

(52) Liu, Y.; Shi, L.; Su, L.; van der Mei, H. C.; Jutte, P. C.; Ren, Y.; Busscher, H. J. Nanotechnology-based Antimicrobials and Delivery Systems for Biofilm-infection Control. *Chem. Soc. Rev.* **2019**, *48*, 428−446.

(53) Dai, X.; Zhao, Y.; Yu, Y.; Chen, X.; Wei, X.; Zhang, X.; Li, C. All-in-one NIR-activated Nanoplatforms for Enhanced Bacterial Biofilm Eradication. *Nanoscale* **2018**, *10*, 18520−18530.

(54) Li, J.; Zhang, K.; Ruan, L.; Chin, S. F.; Wickramasinghe, N.; Liu, H.; Ravikumar, V.; Ren, J.; Duan, H.; Yang, L.; Chan-Park, M. B. Block Copolymer Nanoparticles Remove Biofilms of Drug-Resistant Gram-Positive Bacteria by Nanoscale Bacterial Debridement. *Nano Lett.* **2018**, *18*, 4180−4187.